

Size-dependent critical localization

Hui-Qiang Liang,¹ Linhu Li,^{2,*} and Guo-Fu Xu^{1,†}

¹Department of Physics, Shandong University, Jinan 250100, China

²Quantum Science Center of Guangdong-Hong Kong-Macao Greater Bay Area (Guangdong), Shenzhen, China

(Dated: September 26, 2025)

Studying critical states in quasiperiodic systems is of great importance in localization physics. Previously identified critical states share a common characteristic: they exhibit persistent critical features in the thermodynamic limit. In this Letter, we predict an exotic type of critical states, termed size-dependent critical states, which exhibit a fundamentally distinct behavior. Specifically, they display critical localization signatures only at finite sizes, but transition to Anderson localization in the thermodynamic limit. We establish that the physical origin of size-dependent critical states lies in the synergistic interplay between local non-reciprocal domain walls and non-Hermitian skin effects. By revealing a critical phase that challenges the established paradigm of critical localization, our work opens new avenues for exploring localization phenomena in quasiperiodic systems.

Introduction.— In localization physics [1–4], the study of critical states in quasiperiodic systems is fundamentally important and attracts considerable attention. Within Hermitian quasiperiodic systems, critical states intermediate between extended and localized states and often exhibit intriguing properties [5–33]. For instance, they demonstrate multifractality, characterized by pronounced intensity fluctuations across the system and describable by an infinite set of fractal dimensions. Furthermore, their associated energy spectrum is singular continuous: neither pure point (typical of localized states) nor absolutely continuous (typical of extended states). This means it has zero Lebesgue measure – containing no continuous energy intervals – yet is not composed solely of discrete eigenvalues.

While critical states in Hermitian quasiperiodic systems have been extensively studied, research has significantly expanded to explore their counterparts in non-Hermitian quasiperiodic systems. It is known that non-Hermitian systems host many exotic features [34–47], such as the famous non-Hermitian skin effect (NHSE) induced by non-reciprocal hoppings, the generally complex eigenvalues with the imaginary part directly signifying exponential growth or decay of states over time, and the unique spectral degeneracies where not only eigenvalues but also eigenvectors coalesce. These exotic features impart novel characteristics to critical states in non-Hermitian quasiperiodic systems [48–52], such as complex mobility rings [53] and skin-like critical states [54], garnering growing interest.

Despite these differences, previously identified critical states in both Hermitian and non-Hermitian quasiperiodic systems share a common characteristic: their critical features persist robustly in the thermodynamic limit. For clarity, we hereafter refer to such states as conventional critical states and their behavior can be seen from Fig. 1(a). In this Letter, we predict an exotic type of critical states, termed size-dependent critical (SDC) states, which exhibit a fundamentally distinct behavior from conventional critical states. As shown in Fig. 1(b), they exhibit critical localization exclusively at finite sizes, but undergo a transition to Anderson localization in the thermodynamic limit. Using Lyapunov exponent (LE) analysis and multifractal analysis, we identify three types of eigenstates in an mosaic lattice with non-

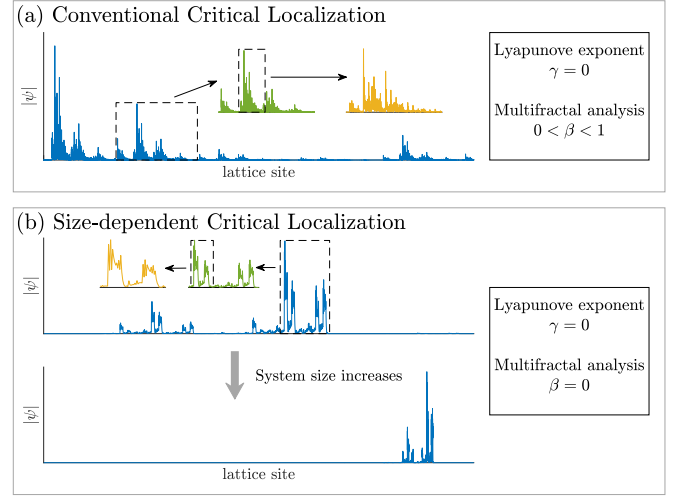


FIG. 1. (a) Conventional critical localization: The wavefunction possesses self-similarity, characteristic of multifractality. (b) Size-dependent critical localization: The wavefunction exhibits critical behavior only at finite sizes, crossing over to a localized state in the thermodynamic limit.

reciprocal hopping: Anderson-localized states, conventional critical states, and SDC states. We then employ entanglement entropy to examine the size-dependent characteristic of the SDC states, confirming the existence of critical sizes. We also establish that the physical origin of SDC states lies in the synergic interplay between local non-reciprocal domain walls (DWs) and NHSEs. Since our work reveals a novel type of critical states that challenge the established paradigm of critical localization, it opens new avenues for exploring localization phenomena in quasiperiodic systems.

The model.— To demonstrate SDC states, we consider a mosaic model incorporating non-reciprocal hopping, under closed boundary conditions, as depicted in Fig. 2(a). Its Hermitian part without non-reciprocal hopping, which hosts critical states protected by incommensurately distributed zeros within its hopping terms, is given by [20]

$$H_0 = \sum_j (t_j \hat{a}_j^\dagger \hat{a}_{j+1} + \text{H.c.}) + \sum_j V_j \hat{a}_j^\dagger \hat{a}_j, \quad (1)$$

where \hat{a}_j^\dagger (\hat{a}_j) is the creation (annihilation) operator associated with the j -th site, with $j = 1, \dots, L$. The quasiperiodic hopping coefficient t_j and on-site potential V_j are mosaic, with

$$\{t_j, V_j\} = \begin{cases} \{\lambda, 2t_0 \cos(2\pi\alpha(j-1) + \theta)\}, & j = 1 \bmod \kappa, \\ 2t_0 \cos(2\pi\alpha j + \theta)\{1, 1\}, & j = 0 \bmod \kappa, \\ \{\lambda, 0\}, & \text{else.} \end{cases} \quad (2)$$

Here, λ and θ denote the hopping coefficient and phase offset, respectively, and $t_0 = 1$ is set as the energy unit. $\kappa \geq 2$ is an integer representing how many lattice sites are within a quasicell, that is, $L = \kappa N$ with N representing the number of quasicells. For simplicity, here we focus on the model with $\kappa = 2$; extensions of our results to general values of κ can be found in Supplemental Materials S1. The quasiperiodic modulation is described by an irrational number α , chosen as $\alpha = \lim_{m \rightarrow \infty} (F_{m-1}/F_m) = (\sqrt{5}-1)/2$, where F_m are Fibonacci numbers defined recursively by $F_{m+1} = F_{m-1} + F_m$, starting from $F_0 = F_1 = 1$. In finite systems, one may choose the number of quasicells N as F_m and take the rational approximation $\alpha \approx \alpha_m = F_{m-1}/F_m$.

Next, we introduce non-reciprocal hoppings to the mosaic model, and the total Hamiltonian is given by

$$H = H_0 + \sum_{j=0 \bmod \kappa} (h \hat{a}_j^\dagger \hat{a}_{j+1} - h \hat{a}_{j+1}^\dagger \hat{a}_j) + \sum_{j \neq 0 \bmod \kappa} (g \hat{a}_j^\dagger \hat{a}_{j+1} - g \hat{a}_{j+1}^\dagger \hat{a}_j), \quad (3)$$

where h ($h < 2t_0$) and g ($g < \lambda$) control the magnitudes of the non-reciprocity. As shown in Fig. 2(b), the eigenenergies of H can be divided into three categories (labeled I, II, and III) according to their spectral characteristics and the fractal dimension (FD) Γ_n of the corresponding eigenstate, where $\Gamma_n = -\ln[\sum_{j=1}^L |\psi_{j,n}|^4] / \ln L$ with $\psi_{j,n}$ the amplitude of the n -th eigenstate at the j -th lattice site. We accordingly designate the associated eigenstates as types I, II, and III eigenstates.

As shown in Fig. 2(c), type I eigenstates exhibit Anderson localization induced by the quasiperiodic modulation. Moreover, Fig. 2(b) shows that the strong localization (indicated by $\text{FD} \approx 0$) of these states blocks any possible non-reciprocity current even when the boundaries are closed, as reflected by their line spectrum with zero interior [42]. In contrast, Fig. 2(d) shows that type II eigenstates exhibit a relatively extended distribution ($0 \ll \text{FD} < 1$), reminiscent of fractal structures of critical states. Since these states distribute across the whole lattice, they experience a global non-reciprocal current that leads to loop-like spectrum when the boundaries are closed [42], as shown in Fig. 2(b). Note that these states transform into skin states with line-like spectrum when the boundaries are open, which cuts off the non-reciprocal current [see Supplemental Materials S2]. Most intriguingly, Fig. 2(e) shows that type III eigenstates display similar fractal features and distribute across the lattice as type II eigenstates. However, Fig. 2(b) shows that their line-like spectrum indicates the absence of a global non-reciprocal current, suggesting an exotic mixture of types I and II scenarios.

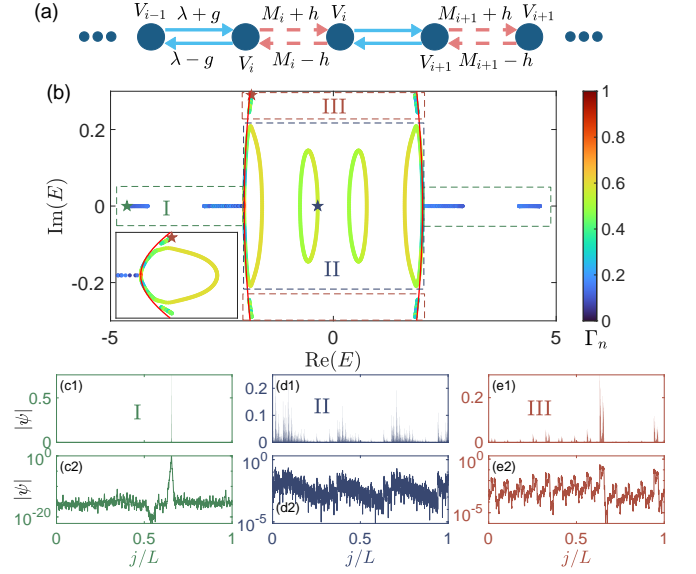


FIG. 2. (a) The non-Hermitian quasiperiodic mosaic model with $\kappa = 2$. The solid circles denote the lattice sites, V_i is the quasiperiodic mosaic potential, and the red dotted and blue arrows denote the quasiperiodic hopping ($M_i \pm h$) and constant hopping ($\lambda \pm g$) respectively, where $M_i = V_i = 2t_0 \cos(2\pi\kappa\alpha i)$ at the i -th quasicell. (b) The eigenenergies of H and the associated FDs. (c-e) display the characteristic spatial profiles of types I, II and III eigenstates, respectively. Other parameters are $\lambda = 2$, $h = 0.7$, $g = 0.73$, $\theta = 0$, and $N = 987$.

The characteristics of the eigenstates.—To characterize the criticality of the eigenstates, we employ LE analysis and multifractal analysis. LE serves as a highly effective metric for quantifying eigenstate localization, calculable via transfer matrices. In our case, for an eigenstate with energy E , the corresponding LE reads $\gamma_\epsilon(E) = \lim_{N \rightarrow \infty} \frac{1}{2\pi N} \int \ln \|\mathcal{T}_{N,1}(\theta + i\epsilon)\| d\theta$. In the above, $\mathcal{T}_{N,1} = \prod_{i=1}^N \mathcal{T}_i = \mathcal{T}_N \mathcal{T}_{N-1} \cdots \mathcal{T}_2 \mathcal{T}_1$, N is the number of quasicells, $\|\cdot\|$ denotes the square root of the largest eigenvalue of the matrix, and ϵ is the imaginary part of the complexified θ , where $\mathcal{T}_i = T_{j_0+\kappa} T_{j_0+\kappa-1} \cdots T_{j_0}$ is the transfer matrix of the i -th quasicell, with T_j the transfer matrix of the j -th lattice site, i.e., $(\psi_{j+1}, \psi_j)^T = T_j(\psi_j, \psi_{j-1})^T$, and j_0 the first site of per quasicell. Using Avila's global theory [55], the LE $\gamma_\epsilon(E)$ becomes ϵ -independent, and reads [20, 56]

$$\gamma(E) = \max \left\{ \frac{1}{2} \ln \left| \frac{E}{\lambda + g} \right| + \sqrt{\left(\frac{E}{\lambda + g} \right)^2 - \frac{\lambda - g}{\lambda + g}}, 0 \right\}. \quad (4)$$

The mobility ring can be determined by the solution of

$$\left| \frac{E}{\lambda + g} \right| + \sqrt{\left(\frac{E}{\lambda + g} \right)^2 - \frac{\lambda - g}{\lambda + g}} = 1. \quad (5)$$

The mobility ring is a loop centered at the origin in the complex energy plane, separating regions with $\gamma(E) > 0$ and those with $\gamma(E) = 0$, where $\gamma(E) > 0$ means the corresponding eigenstates are localized, and $\gamma(E) = 0$ indicates delocalized

states with infinite localization lengths, a characteristic of extended or critical states. As shown in Fig. 2(b), type I eigenstates fall outside the mobility ring and thereby their LEs are given by $\gamma(E) > 0$, consistent with their localized distributions discussed previously. On the other hand, types II and III eigenstates are inside the mobility ring and have $\gamma(E) = 0$, suggesting they are either extended or critical states.

We next apply multifractal analysis [17] to unveil the distinction between types II and III eigenstates. For an eigenstate $|\psi_n\rangle$, a scaling exponent $\beta_{j,n}$ can be extracted from the on-site probability $P_{j,n} = |\psi_{j,n}|^2 \sim \left(\frac{1}{F_m}\right)^{\beta_{j,n}}$, where $\psi_{j,n}$ is the amplitude of $|\psi_n\rangle$ at site j . According to multifractal analysis, when the eigenstate $|\psi_n\rangle$ is extended, the maximum of $P_{j,n}$ over j scales as $\max_j(P_{j,n}) \sim 1/F_m$, and $\beta_{\min,n} \equiv \min_j(\beta_{j,n}) = 1$. For a localized eigenstate $|\psi_n\rangle$, $P_{j,n}$ peaks at very few sites and is nearly zero at the other sites, yielding $\max_j(P_{j,n}) \sim \text{constant}$ and $\beta_{\min,n} = 0$. Finally, $\beta_{\min,n}$ for a critical eigenstate $|\psi_n\rangle$ falls within the interval $(0, 1)$. To reduce fluctuations, we use the average scaling exponent, defined by

$$\beta_{\min} = \frac{1}{L'} \sum_n \beta_{\min,n}, \quad (6)$$

to characterize the three types of eigenstates, where L' denotes the number of eigenstates of the same type (type I, II, or III), and the summation runs over these states.

Fig. 3 shows the average scaling exponents β_{\min} for the three types of eigenstates, as a function of the inverse Fibonacci index $1/m$ that determines the system size through $L = \kappa F_m$ in our consideration. In consistence with the LE analysis, the average scaling exponents β_{\min} for types I and II eigenstates asymptotically tend to zero and have a finite value in the thermodynamic limit ($1/m \rightarrow 0$), which indicates their localized and critical natures, respectively. In comparison, β_{\min} of type III eigenstates asymptotically tends to zero when $1/m \rightarrow 0$, indicating their localized nature in the thermodynamic limit. β_{\min} of type III eigenstates can take values larger than that of type II eigenstates but much smaller than 1 when $1/m \gtrsim 0.07$, suggesting a critical behavior of these states at finite sizes. Indeed, our LE analysis shows that these states have $\gamma(E) = 0$ and fall inside the mobility ring for a finite-size system, verifying their SDC behaviors.

The size-dependent feature.— To verify the size-dependency of type III eigenstates, we analyze their biorthogonal entanglement entropy [41, 57–59] as a function of system sizes. Specifically, we choose an entanglement partition between the left and right halves of the lattice (i.e., sites with $[1, L/2]$ and $[L/2 + 1, L]$), and the entanglement entropy is given by

$$S_n = - \sum_p \zeta_{p,n} \ln \zeta_{p,n} + (1 - \zeta_{p,n}) \ln(1 - \zeta_{p,n}), \quad (7)$$

where $\zeta_{p,n}$ denotes the p -th eigenvalue of the correlator matrix C_n , whose x, y entry is defined by $(C_n)_{xy} = \langle \psi_n | \hat{a}_x^\dagger \hat{a}_y | \psi_n \rangle$, with $|\psi_n\rangle$ the n -th eigenstate and $x, y \in [1, L/2]$.

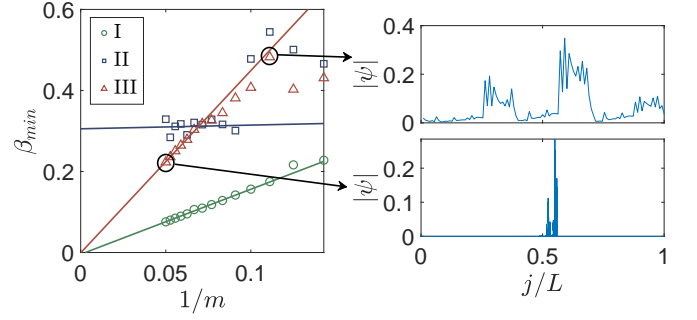


FIG. 3. Left panel: The average scaling exponents β_{\min} as a function of the inverse Fibonacci index $1/m$ for the three types of eigenstates. $h = g = 0.75$ and the other parameters are the same as those in Fig. 2. Here the linear fit for type III eigenstates is obtained from the results with $m > 13$ to show their asymptotical behavior in the thermodynamical limit; for smaller m , β_{\min} for type III eigenstates deviates away from the linear fit and remains much less than 1. Right panels: The wavefunction distributions of typical SDC states.

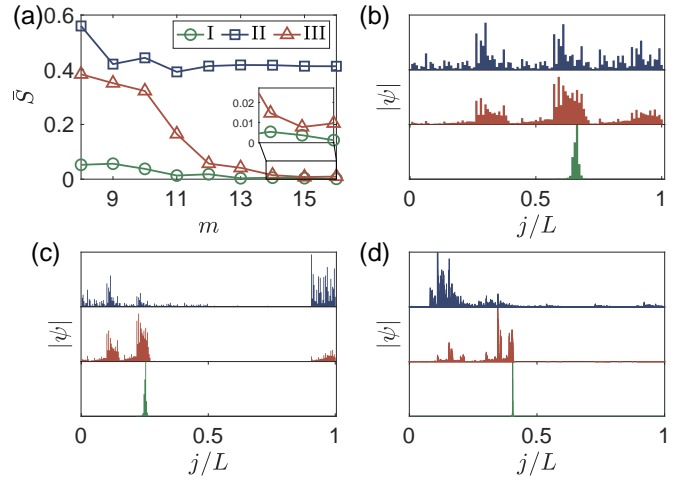


FIG. 4. (a) The average entanglement entropies as a function of the Fibonacci index m . (b-d) The distributions of the eigenstates with m respectively being 9, 11, 16. For (b-d), each comprises three panels: from top to bottom, they respectively exhibit the distribution of the conventional critical state (the $L/2$ -th eigenstate), that of the size-dependent critical states (the eigenstate with the maximum imaginary energy), and that of the localized state (the first eigenstate). Here, we sort the eigenstates by the real parts of their energies. The parameters are the same as those in Fig. 2 except for $h = g = 0.75$.

Fig. 4 shows the entanglement entropy averaged over each of the three types of eigenstates, $\bar{S} = \sum_n S_n / L'$, where type III eigenstates show a clear size-dependence in comparison with the others. Explicitly, $\bar{S} \approx 0$ is seen for type I eigenstates, corresponding to the non-ergodic nature of localized states; while type II eigenstates have a finite \bar{S} smaller than its possible maximum $\ln 2$, corresponding to the partially ergodic nature of critical states with approximately extended distributions. In contrast, \bar{S} of type III eigenstates takes a finite value close to that of type II at small system sizes, but drops toward

zero as the system size increases, showing a size-dependent transition between partially ergodic and non-ergodic states at a critical size L_c corresponding to $m = 12$ in our numerics. In Figs. 4(b) to (d), we display the wave amplitudes of the three types of eigenstates with different system sizes, where types I and II eigenstates show size-independent localized and critical distributions, respectively. Meanwhile, type III eigenstates are seen to possess nonzero distribution across the system when $L < L_c$ [Figs. 4(b) and (c)], indicating their partial ergodic and critical behaviors. However, as shown in Fig. 4(d), wave amplitudes of type III eigenstate drastically drop to zero at most sites when $L > L_c$, indicating a non-ergodic localized feature. This size-dependent localization transition is unambiguously captured by the finite-size scaling of the average entanglement entropy, confirming that type III eigenstates are SDC states.

The physical origin of SDC states.— To elucidate the physical origin of SDC states, we first examine the mosaic model without non-reciprocal hopping, governed by the Hamiltonian H_0 . Previous research has established that this model hosts precise energy-dependent mobility edges separating localized and critical states, expressed as $|E| = \lambda$ [20]. Further introducing non-reciprocity to hopping parameters may alter the distribution properties of eigenstates. In our model, the non-reciprocity is described by two parameters h and g in Eq. (3). To clarify the origin of SDC states, we first consider the case where $h \neq 0$ and $g = 0$, followed by the case where both h and g are nonzero.

As seen from Figs. 5(a1) and (a2), adding a nonzero h to the Hermitian Hamiltonian H_0 assigns complex eigenenergies to eigenstates of H_0 outside (but close to) the mobility edges $|E| = \lambda = 2$. Furthermore, in the above process, one can see that the real eigenvalues coalesce at an exceptional point and subsequently split into complex-conjugate pairs with imaginary components of opposite signs, indicating the pseudo-Hermitian phase transition. After this transition, critical and Anderson states (with real energies inside and outside the mobility edges, respectively) also coalesce into states with relatively weaker localization, as shown by the inverse participation ratios of two typical eigenstates in Fig. 5(a3).

To understand their origin, we define the local non-reciprocity δ_j and the average hopping amplitude η_j ,

$$\delta_j = \ln \left| \frac{t_j + h}{t_j - h} \right|, \quad \eta_j = \sqrt{|(t_j + h)(t_j - h)|}, \quad (8)$$

where $j \bmod \kappa = 0$. Explicitly, the sign of δ_j describes the non-reciprocal direction (towards the left when $\delta_j > 0$), and its absolute value describes the net non-reciprocal strength; while η_j describes the degree of coupling between two lattice sites connected by $t_j \pm h$. Note that besides the fully decoupled case with $(t_j, h) = 0$, the condition $t_j = \pm h$ also indicates another effectively decoupled scenario, where the two-site system is at an exceptional point and thus possesses a single eigenstate distributed only on one lattice site. In Figs. 5(b1) and (b2), it is seen that η_j oscillates with a quasi-period of roughly 30 ~ 40 lattice sites. Eigenstates with complex energies are found to localize around multiple positions where η_j

shows the strongest fluctuation. These localization centers coincide with DWs where δ_j undergoes sign reversal, indicating their origin of local non-reciprocal DWs. Such a multi-center localization explains the weaker localization after the pseudo-Hermitian transition.

We now consider the case where $h \neq 0$ and $g \neq 0$. The parameter g represents a uniform non-reciprocal pumping throughout the system, which can induce a NHSE for type II eigenstates under open boundary conditions. Physically, such a global non-reciprocal pumping tends to suppress the localization induced by the local hopping oscillation from t_j and non-reciprocity from nonzero h . Indeed, increasing h enlarges the MR that encloses the critical region, as shown in Fig. 5(c). Simultaneously, Anderson states with complex eigenenergies are gradually pushed towards the MR, transitioning to (size-dependent) critical states when their eigenenergies eventually fall inside the MR, as shown in Figs. 5(d) and (e). Finally, further increasing h merges these states into type II eigenstates with conventional criticality, as shown in Fig. 5(f).

Figs. 5(g) and (h) show the entanglement entropy S_n of the eigenstate with the maximum imaginary energy at different sizes $m = 9$ and $m = 16$, respectively. It is seen that SDC states appear around the transition between regions with conventional critical states ($S_n \approx \ln 2$) and Anderson states ($S_n \approx 0$), indicated by the region with intermediate values of S_n for a relatively smaller system size that disappears when the size increases to $m = 16$. We further note that the SDC localization is expected to be a general phenomenon in one-dimensional non-Hermitian quasiperiodic lattices which host critical localization as well as local non-reciprocal DWs and NHSEs. As an additional example, in Supplemental Materials S3, SDC localization is shown to arise also in a non-reciprocal Aubry-Andre model [60].

Conclusion.— We have predicted a novel type of critical states, termed SDC states, exhibiting behavior fundamentally distinct from conventional critical states. While conventional critical states persist critical features in the thermodynamic limit, SDC states exhibit critical localization signatures only at finite sizes, transitioning to Anderson localization in the thermodynamic limit. Using a non-reciprocal hopping mosaic model, the size-dependent features of these states are confirmed by analyzing the entanglement entropy of them at different sizes. We establish that the physical origin of SDC states lies in the synergistic interplay between local non-reciprocal DWs and NHSEs: the mosaic model with inhomogeneous non-reciprocal hopping hosts eigenstates near the mobility edge, which are weakly localized at local non-reciprocal DWs; subsequent action of NHSEs converts these weakly localized states into SDC states. SDC localization challenges conventional paradigms and understandings of critical localization, offering fresh insights into skin-induced phenomena in quasiperiodic systems. It unlocks new possibilities for multifractal wave manipulation and control in engineered systems, while inviting further investigations and potential extensions to interacting systems where interacting phases with size-dependent features can arise [13, 61–63].

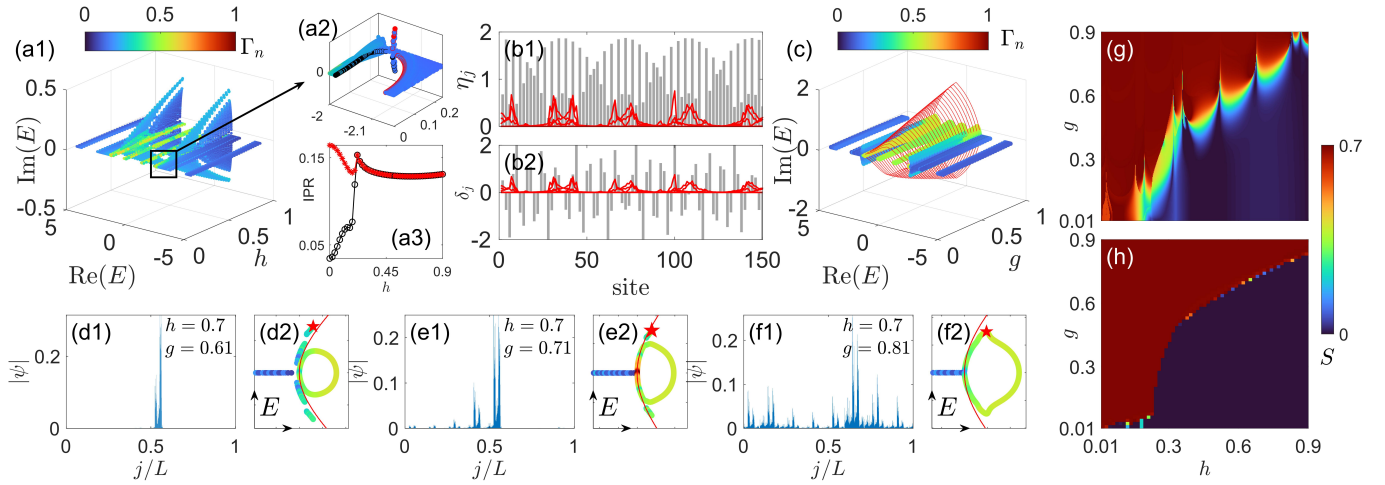


FIG. 5. (a1,a2) FDs of different eigenstates as a function of E and h for $g = 0$ and $N = 1597$. (a3) The inverse participation ratios, $\sum_j |\psi_{jn}|^4$, of the eigenstates marked by red and black dots in (a2). (b) The local non-reciprocity δ_j and the average hopping amplitude η_j for $h = 0.7$, $g = 0$, and $j \bmod \kappa = 0$. Red lines: the distributions of wavefunctions with $|\text{Re}(E)| > 1.9$ and $\text{Im}(E) > 0$. (c) FDs of different eigenstates as a function of E and g for $h = 0.7$ and $N = 1597$. Red loops: the MRs (Eq. (5)). (d-f) The eigenspectrum, the MR (red line) and the distribution of wavefunction (the corresponding eigenenergy marked by red star in the spectrum) for $h = 0.7$, $g = 0.61, 71, 81$. (g) and (h) are g - h phase diagram of the eigenstates with $\max(\text{Im}(E))$ for sizes $m = 9$ and $m = 16$, respectively. Other parameters are $\lambda = 2$, $\kappa = 2$, (a) $N = 144$, and (d-f) $N = 987$.

Acknowledgments. L.L. acknowledges support from the National Natural Science Foundation of China through Grant No. 12474159. G.-F.X. acknowledges support from the National Natural Science Foundation of China through Grant No. 12174224, and Shandong Provincial Natural Science Foundation of China through Grant No. ZR2023MA048.

* lilinhu@quantumsc.cn
† xgf@sdu.edu.cn

- [1] P. W. Anderson, Absence of diffusion in certain random lattices, *Phys. Rev.* **109**, 1492 (1958).
- [2] K. Ishii, Localization of eigenstates and transport phenomena in the one-dimensional disordered system, *Suppl. Prog. Theor. Phys.* **53**, 77 (1973).
- [3] D. Thouless, Electrons in disordered systems and the theory of localization, *Phys. Rep.* **13**, 93 (1974).
- [4] F. Evers and A. D. Mirlin, Anderson transitions, *Rev. Mod. Phys.* **80**, 1355 (2008).
- [5] Y. Hatsugai and M. Kohmoto, Energy spectrum and the quantum hall effect on the square lattice with next-nearest-neighbor hopping, *Phys. Rev. B* **42**, 8282 (1990).
- [6] J. H. Han, D. J. Thouless, H. Hiramoto, and M. Kohmoto, Critical and bicritical properties of harper's equation with next-nearest-neighbor coupling, *Phys. Rev. B* **50**, 11365 (1994).
- [7] D. Tanese, E. Gurevich, F. Baboux, T. Jacqmin, A. Lemaître, E. Galopin, I. Sagnes, A. Amo, J. Bloch, and E. Akkermans, Fractal energy spectrum of a polariton gas in a fibonacci quasiperiodic potential, *Phys. Rev. Lett.* **112**, 146404 (2014).
- [8] F. Liu, S. Ghosh, and Y. D. Chong, Localization and adiabatic pumping in a generalized aubry-andré-harper model, *Phys. Rev. B* **91**, 014108 (2015).
- [9] Q.-B. Zeng, S. Chen, and R. Lü, Generalized aubry-andré-harper model with p -wave superconducting pairing, *Phys. Rev. B* **94**, 125408 (2016).
- [10] J. Wang, X.-J. Liu, G. Xianlong, and H. Hu, Phase diagram of a non-abelian aubry-andré-harper model with p -wave superfluidity, *Phys. Rev. B* **93**, 104504 (2016).
- [11] C. Yang, Y. Wang, P. Wang, X. Gao, and S. Chen, Dynamical signature of localization-delocalization transition in a one-dimensional incommensurate lattice, *Phys. Rev. B* **95**, 184201 (2017).
- [12] H. Yao, A. Khoudli, L. Bresque, and L. Sanchez-Palencia, Critical behavior and fractality in shallow one-dimensional quasiperiodic potentials, *Phys. Rev. Lett.* **123**, 070405 (2019).
- [13] Y. Wang, L. Zhang, S. Niu, D. Yu, and X.-J. Liu, Realization and detection of nonergodic critical phases in an optical raman lattice, *Phys. Rev. Lett.* **125**, 073204 (2020).
- [14] V. Goblot, A. Štrkalj, N. Pernet, J. L. Lado, C. Dorow, A. Lemaître, L. Le Gratiet, A. Harouri, I. Sagnes, S. Ravets, *et al.*, Emergence of criticality through a cascade of delocalization transitions in quasiperiodic chains, *Nat. Phys.* **16**, 832 (2020).
- [15] T. Xiao, D. Xie, Z. Dong, T. Chen, W. Yi, and B. Yan, Observation of topological phase with critical localization in a quasiperiodic lattice, *Science Bulletin* **66**, 2175 (2021).
- [16] X. Tong, Y.-M. Meng, X. Jiang, C. Lee, G. D. d. M. Neto, and G. Xianlong, Dynamics of a quantum phase transition in the aubry-andré-harper model with p -wave superconductivity, *Phys. Rev. B* **103**, 104202 (2021).
- [17] T. Liu, X. Xia, S. Longhi, and L. Sanchez-Palencia, Anomalous mobility edges in one-dimensional quasiperiodic models, *SciPost Phys.* **12**, 027 (2022).
- [18] Y. Wang, L. Zhang, W. Sun, T.-F. J. Poon, and X.-J. Liu, Quantum phase with coexisting localized, extended, and critical zones, *Phys. Rev. B* **106**, L140203 (2022).
- [19] M. Gonçalves, B. Amorim, E. V. Castro, and P. Ribeiro, Criti-

- cal phase dualities in 1d exactly solvable quasiperiodic models, *Phys. Rev. Lett.* **131**, 186303 (2023).
- [20] X.-C. Zhou, Y. Wang, T.-F. J. Poon, Q. Zhou, and X.-J. Liu, Exact new mobility edges between critical and localized states, *Phys. Rev. Lett.* **131**, 176401 (2023).
- [21] H. Li, Y.-Y. Wang, Y.-H. Shi, K. Huang, X. Song, G.-H. Liang, Z.-Y. Mei, B. Zhou, H. Zhang, J.-C. Zhang, *et al.*, Observation of critical phase transition in a generalized aubry-andré-harper model with superconducting circuits, *npj Quantum Information* **9**, 40 (2023).
- [22] X. Lin, X. Chen, G.-C. Guo, and M. Gong, General approach to the critical phase with coupled quasiperiodic chains, *Phys. Rev. B* **108**, 174206 (2023).
- [23] S. Lee, A. Andreanov, and S. Flach, Critical-to-insulator transitions and fractality edges in perturbed flat bands, *Phys. Rev. B* **107**, 014204 (2023).
- [24] Q. Dai, Z. Lu, and Z. Xu, Emergence of multifractality through cascadelike transitions in a mosaic interpolating aubry-andré-fibonacci chain, *Phys. Rev. B* **108**, 144207 (2023).
- [25] T. Shimasaki, M. Prichard, H. E. Kondakci, J. E. Pagett, Y. Bai, P. Dotti, A. Cao, A. R. Dardia, T.-C. Lu, T. Grover, *et al.*, Anomalous localization in a kicked quasicrystal, *Nat. Phys.* **20**, 409 (2024).
- [26] X. Li, H. Xu, J. Wang, L.-Z. Tang, D.-W. Zhang, C. Yang, T. Su, C. Wang, Z. Mi, W. Sun, X. Liang, M. Chen, C. Li, Y. Zhang, K. Linghu, J. Han, W. Liu, Y. Feng, P. Liu, G. Xue, J. Zhang, Y. Jin, S.-L. Zhu, H. Yu, S. P. Zhao, and Q.-K. Xue, Mapping the topology-localization phase diagram with quasiperiodic disorder using a programmable superconducting simulator, *Phys. Rev. Res.* **6**, L042038 (2024).
- [27] W. Chen, P. D. Sacramento, and R. Mondaini, Multifractality and prethermalization in the quasiperiodically kicked aubry-andré-harper model, *Phys. Rev. B* **109**, 054202 (2024).
- [28] C. Guo, Multiple intermediate phases in the interpolating aubry-andré-fibonacci model, *Phys. Rev. B* **109**, 174203 (2024).
- [29] C. Yang, W. Yang, Y. Wang, and Y. Wang, Exploring multifractal critical phases in two-dimensional quasiperiodic systems, *Phys. Rev. A* **110**, 042205 (2024).
- [30] C. W. Duncan, Critical states and anomalous mobility edges in two-dimensional diagonal quasicrystals, *Phys. Rev. B* **109**, 014210 (2024).
- [31] Q. Yao, X. Yang, A. A. Iliasov, M. I. Katsnelson, and S. Yuan, Wave functions in the critical phase: A planar sierpinski fractal lattice, *Phys. Rev. B* **110**, 035403 (2024).
- [32] Y. Bai and D. M. Weld, Tunably polarized driving light controls the phase diagram of one-dimensional quasicrystals and two-dimensional quantum hall matter, *Phys. Rev. B* **111**, 115163 (2025).
- [33] P. Dotti, Y. Bai, T. Shimasaki, A. R. Dardia, and D. M. Weld, Measuring a localization phase diagram controlled by the interplay of disorder and driving, *Phys. Rev. Res.* **7**, L022026 (2025).
- [34] T. E. Lee, Anomalous edge state in a non-hermitian lattice, *Phys. Rev. Lett.* **116**, 133903 (2016).
- [35] C. H. Lee and R. Thomale, Anatomy of skin modes and topology in non-hermitian systems, *Phys. Rev. B* **99**, 201103 (2019).
- [36] S. Yao and Z. Wang, Edge states and topological invariants of non-hermitian systems, *Phys. Rev. Lett.* **121**, 086803 (2018).
- [37] K. Yokomizo and S. Murakami, Non-bloch band theory of non-hermitian systems, *Phys. Rev. Lett.* **123**, 066404 (2019).
- [38] D. S. Borgnia, A. J. Kruchkov, and R.-J. Slager, Non-hermitian boundary modes and topology, *Phys. Rev. Lett.* **124**, 056802 (2020).
- [39] N. Okuma, K. Kawabata, K. Shiozaki, and M. Sato, Topological origin of non-hermitian skin effects, *Phys. Rev. Lett.* **124**, 086801 (2020).
- [40] Y. Ashida, Z. Gong, and M. Ueda, Non-hermitian physics, *Adv. Phys.* **69**, 249 (2020).
- [41] L. Li, C. H. Lee, S. Mu, and J. Gong, Critical non-hermitian skin effect, *Nat. Commun.* **11**, 5491 (2020).
- [42] K. Zhang, Z. Yang, and C. Fang, Correspondence between winding numbers and skin modes in non-hermitian systems, *Phys. Rev. Lett.* **125**, 126402 (2020).
- [43] P. Delplace, T. Yoshida, and Y. Hatsugai, Symmetry-protected multifold exceptional points and their topological characterization, *Phys. Rev. Lett.* **127**, 186602 (2021).
- [44] I. Mandal and E. J. Bergholtz, Symmetry and higher-order exceptional points, *Phys. Rev. Lett.* **127**, 186601 (2021).
- [45] K. Zhang, Z. Yang, and C. Fang, Universal non-hermitian skin effect in two and higher dimensions, *Nat. Commun.* **13**, 2496 (2022).
- [46] S. Longhi, Erratic non-hermitian skin localization, *Phys. Rev. Lett.* **134**, 196302 (2025).
- [47] T. Yoshida, E. J. Bergholtz, and T. Bzdušek, Hopf exceptional points, arXiv preprint arXiv:2504.13012 10.48550/arXiv.2504.13012 (2025).
- [48] S. Longhi, Phase transitions in a non-hermitian aubry-andré-harper model, *Phys. Rev. B* **103**, 054203 (2021).
- [49] G.-J. Liu, J.-M. Zhang, S.-Z. Li, and Z. Li, Emergent strength-dependent scale-free mobility edge in a nonreciprocal long-range aubry-andré-harper model, *Phys. Rev. A* **110**, 012222 (2024).
- [50] Y.-Q. Zheng, S.-Z. Li, and Z. Li, Emergent multiloop nested point gap in a non-hermitian quasiperiodic lattice, *Phys. Rev. B* **111**, 104204 (2025).
- [51] Y.-J. Zhao, H.-Z. Li, X. Huang, S.-Z. Li, and J.-X. Zhong, Fate of pseudomobility edges and multiple states in a non-hermitian wannier-stark lattice, *Phys. Rev. B* **111**, 014315 (2025).
- [52] J.-L. Dong, E.-W. Liang, S.-Y. Liu, G.-Q. Zhang, L.-Z. Tang, and D.-W. Zhang, Critical properties in the non-hermitian aubry-andré-stark model, *Phys. Rev. B* **111**, 174209 (2025).
- [53] S.-Z. Li and Z. Li, Ring structure in the complex plane: A fingerprint of a non-hermitian mobility edge, *Phys. Rev. B* **110**, L041102 (2024).
- [54] X. Cai, Localization transitions and winding numbers for non-hermitian aubry-andré-harper models with off-diagonal modulations, *Phys. Rev. B* **106**, 214207 (2022).
- [55] A. Avila, Global theory of one-frequency Schrödinger operators, *Acta. Math.* **215**, 1 (2015).
- [56] See Section S1 of the Supplemental Material for the additional details..
- [57] P.-Y. Chang, J.-S. You, X. Wen, and S. Ryu, Entanglement spectrum and entropy in topological non-hermitian systems and nonunitary conformal field theory, *Phys. Rev. Res.* **2**, 033069 (2020).
- [58] L. Li and C. H. Lee, Non-hermitian pseudo-gaps, *Sci. Bull.* **67**, 685 (2022).
- [59] H.-Q. Liang, S. Mu, J. Gong, and L. Li, Anomalous hybridization of spectral winding topology in quantized steady-state responses, *Phys. Rev. B* **105**, L241402 (2022).
- [60] S.-Z. Li, E. Cheng, S.-L. Zhu, and Z. Li, Asymmetric transfer matrix analysis of lyapunov exponents in one-dimensional nonreciprocal quasicrystals, *Phys. Rev. B* **110**, 134203 (2024).
- [61] M. Rispoli, A. Lukin, R. Schittko, S. Kim, M. E. Tai, J. Léonard, and M. Greiner, Quantum critical behaviour at the many-body localization transition, *Nature* **573**, 385 (2019).
- [62] Y. Wang, C. Cheng, X.-J. Liu, and D. Yu, Many-body critical phase: Extended and nonthermal, *Phys. Rev. Lett.* **126**, 080602 (2021).

- (2021).
- [63] S. Singha Roy, S. Bandyopadhyay, R. Costa de Almeida, and P. Hauke, Unveiling eigenstate thermalization for non-hermitian systems, *Phys. Rev. Lett.* **134**, 180405 (2025).

Supplemental Materials for “Size-dependent critical localization”

Hui-Qiang Liang,¹ Linhu Li,^{2,*} and Guo-Fu Xu^{1,†}

¹*Department of Physics, Shandong University, Jinan 250100, China*

²*Quantum Science Center of Guangdong-Hong Kong-Macao Greater Bay Area (Guangdong), Shenzhen, China*

(Dated: September 26, 2025)

S1. THE CALCULATION OF THE LYAPUNOV EXPONENT

In this section, we present the calculation of the Lyapunov exponent (LE) of the proposed model for an arbitrary value of κ . Consider the quasiperiodic Schrödinger operator for the model in the main text,

$$(H_{\lambda,\alpha,\theta}\psi)_n = V_n\psi_n + t_n^+\psi_{n+1} + t_{n-1}^-\psi_{n-1}, \quad (1)$$

where

$$V_n(\theta) = \begin{cases} 2t_0 \cos(2\pi\alpha(j-1) + \theta) & j = 1 \bmod \kappa, \\ 2t_0 \cos(2\pi\alpha j + \theta) & j = 0 \bmod \kappa, \\ 0, & \text{else,} \end{cases} \quad (2)$$

and

$$t_n^\pm(\theta) = \begin{cases} 2t_0 \cos(2\pi\alpha j + \theta) \pm h & j = 0 \bmod \kappa, \\ \lambda \pm g & \text{else,} \end{cases} \quad (3)$$

with $\theta \in (0, 2\pi]$, $\lambda \neq 0$ and $h \leq \lambda$. The LE can be calculated through the transfer matrices [1], that is,

$$\gamma_\epsilon(E) = \lim_{L \rightarrow \infty} \frac{1}{2\pi N} \int \ln \|\mathcal{T}_{N,1}(\theta + i\epsilon)\| d\theta, \quad (4)$$

$$\mathcal{T}_{N,1} = \prod_{i=1}^N \mathcal{T}_i = \mathcal{T}_N \mathcal{T}_{N-1} \cdots \mathcal{T}_2 \mathcal{T}_1, \quad \mathcal{T}_i = T_{j_0+\kappa} T_{j_0+\kappa-1} \cdots T_{j_0}, \quad T_j = \begin{pmatrix} \frac{E-V_j}{t_j^-} & \frac{t_{j-1}^-}{t_j^+} \\ 1 & 0 \end{pmatrix}.$$

In the above, $\mathcal{T}_{N,1} = \prod_{i=1}^N \mathcal{T}_i = \mathcal{T}_N \mathcal{T}_{N-1} \cdots \mathcal{T}_2 \mathcal{T}_1$, N is the number of quasicells, $\|\cdot\|$ denotes the square root of the largest eigenvalue of the matrix, and ϵ is the imaginary part of the complexified θ , where $\mathcal{T}_i = T_{j_0+\kappa} T_{j_0+\kappa-1} \cdots T_{j_0}$ is the transfer matrix of the i -th quasicell, with T_j the transfer matrix of the j -th lattice site, i.e., $(\psi_{j+1}, \psi_j)^T = T_j(\psi_j, \psi_{j-1})^T$, and j_0 the first site of per quasicell. In the thermodynamic limit $L \rightarrow \infty$, the extended and critical states have $\gamma = 0$, while the localized states have $\gamma > 0$. The transfer matrix \mathcal{T}_i can be written as

$$\mathcal{T}_i = \frac{\mathcal{T}'_i}{(M+h)(\lambda+g)} = \frac{\begin{pmatrix} a_\kappa & \alpha a_{\kappa-1} \\ a_{\kappa-1} & \alpha a_{\kappa-2} \end{pmatrix}}{(M+h)(\lambda+g)} \times \begin{pmatrix} (E-M)^2 - (M-h)(M+h) & -(E-M)(\lambda-g) \\ (E-M)(\lambda+g) & (\lambda-h)(\lambda+g) \end{pmatrix}, \quad (5)$$

where $a_\kappa = \Delta^{-1}[(\beta+\Delta)/2]^{\kappa-1} - [(\beta-\Delta)/2]^{\kappa-1}$, $\Delta = \sqrt{\beta^2 + 4\alpha}$, $\beta = E/(\lambda+g)$, $\alpha = -(\lambda-g)/(\lambda+g)$ and $M(\theta+i\epsilon) = 2 \cos(\theta+i\epsilon)$. Furthermore, we employ Avila's global theory of one-frequency analytical $SL(2, \mathbb{C})$ cocycle [2]. In the limit $\epsilon \rightarrow \infty$, a direct computation yields

$$\mathcal{T}'_{i,\epsilon \rightarrow \infty} = \begin{pmatrix} a_\kappa & \alpha a_{\kappa-1} \\ a_{\kappa-1} & \alpha a_{\kappa-2} \end{pmatrix} \begin{pmatrix} -2\beta & -\alpha \\ -1 & 0 \end{pmatrix} + O(e^{-\epsilon}). \quad (6)$$

Consequently, we have

$$\begin{aligned} \kappa \gamma_{\epsilon \rightarrow \infty}(E) &= \ln \left\| \mathcal{T}'_{i,\epsilon \rightarrow \infty} \right\| - A + O(\epsilon^{-1}) \\ &= \ln \left| |a_{\kappa+1}| + \sqrt{a_{\kappa+1}^2 - (-\alpha)^{\kappa-1}} \right| - A + O(\epsilon^{-1}). \end{aligned} \quad (7)$$

with

$$A = \frac{1}{2\pi} \int_0^{2\pi} \ln |(h + 2 \cos(\theta + i\epsilon))| d\theta = \begin{cases} \ln \frac{h + \sqrt{h^2 - 4}}{2}, & h > 2, \\ 0, & h \leq 2. \end{cases} \quad (8)$$

In the main text, we consider the case $h < 2t_0$. According to Avila's global theory, $\gamma_\epsilon(E)$ is a convex, piecewise-linear function with respect to ϵ . For energies E within the spectrum, it follows that

$$\kappa\gamma(E) = \max \left\{ \ln \left| |a_{\kappa+1}| + \sqrt{a_{\kappa+1}^2 - (-\alpha)^{\kappa-1}} \right|, 0 \right\}, \quad (9)$$

with $\epsilon = 0$. Since the localization length is given by $\xi = 1/\gamma$, a vanishing LE ($\gamma = 0$), which characterizes extended or critical states, corresponds to an infinite localization length ($\xi \rightarrow \infty$). Consequently, the mobility ring is determined by

$$\left| |a_{\kappa+1}| + \sqrt{a_{\kappa+1}^2 - (-\alpha)^{\kappa-1}} \right| = 1, \quad (10)$$

where $E = E_R + iE_I$, with E_R and E_I representing the real and imaginary parts of the eigenvalue, respectively. For $\kappa = 2$, the mobility ring is given by

$$\left| \frac{E}{\lambda + g} + \sqrt{\left(\frac{E}{\lambda + g} \right)^2 - \frac{\lambda - g}{\lambda + g}} \right| = 1, \quad (11)$$

that is, the mobility ring is a closed loop in the complex energy plane, centered at $(E_R, E_I) = (0, 0)$. The eigenstates associated with energies inside the loop exhibit a LE $\gamma = 0$, corresponding to extended or critical states, whereas those outside the loop have $\gamma > 0$, indicating localized behaviors.

In Fig. 1, we present numerical results for $\kappa = 3$ and $\kappa = 4$. The eigenstates corresponding to energies inside the mobility ring exhibit multifractal behaviors, as shown in Figs. 1(b2) and (d2). Both cases are consistent with the analysis and argument presented in the main text.

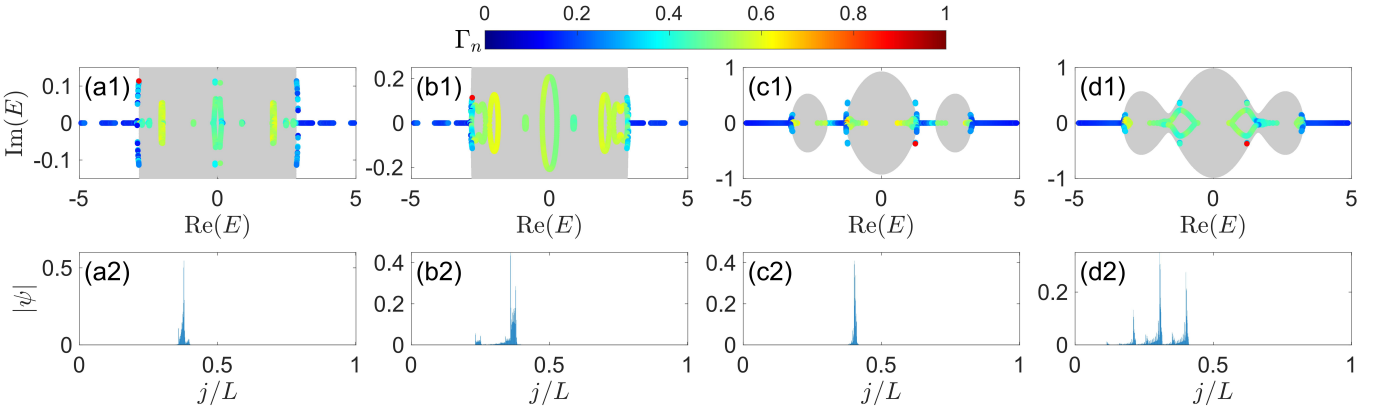


FIG. 1. Fractal dimensions Γ_n of the eigenstates as a function of the complex energy E and the corresponding mobility ring for $\kappa = 3$ (a,b) and $\kappa = 4$ (c,d). Gray regions in the complex energy plane indicate where the LE vanishes ($\gamma = 0$), with their boundaries forming the mobility ring. Wavefunction distributions corresponding to the energies marked in red in (a1, b1, c1, d1) are displayed in (a2, b2, c2, d2), respectively. Parameter values are: (a) $g = 0.1$; (b) $g = 0.4$; (c) $g = 0.1$; (d) $g = 0.3$. Other parameters are fixed at $N = 377$, $\lambda = 2$, and $h = 0.7$.

S2. SIZE-DEPENDENT CRITICAL STATES UNDER OPEN BOUNDARY CONDITIONS

In the main text, we studied size-dependent critical (SDC) states under periodic boundary conditions (PBCs). In this section, we extend our analysis to the spectrum and localization behavior of SDC states under open boundary conditions (OBCs). We adopt the same Hamiltonian parameters as in Eq. (3) of the main text and impose OBCs for this investigation.

As shown in Figs. 2(a) and (b), the conventional critical states transform into skin states under OBCs, and their spectrum no longer retains a loop-like configuration. In contrast, as shown in Figs. 2(a) and (c), the spectrum of the SDC states remains largely unchanged under OBCs. The localization behavior of these SDC states under OBCs can be attributed to the presence of a domain wall in the bulk, which hinders the directional accumulation and reduces the stacking distance.

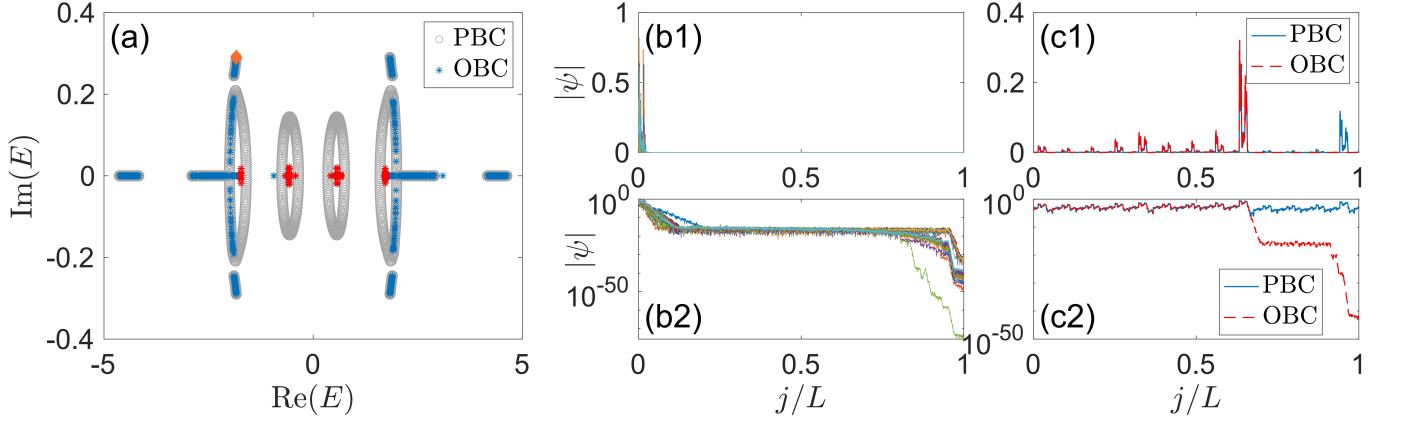


FIG. 2. (a) The spectra under PBCs and OBCs are marked by gray circles and blue asterisks, respectively. The eigenenergies of conventional critical states under OBCs are marked by red asterisks, and the eigenenergies of the SDC states are marked by orange diamonds. (b) The wavefunction distributions of the conventional critical states under OBCs. (c) The wavefunction distributions of the SDC states (their eigenenergies are marked by orange diamonds in (a)). The other parameters are same as those in Fig. 2 of the main text.

S3. SDC STATES IN IRRECIPROCAL AUBRY-ANDRE MODEL

In this section, we study the SDC states in an irreciprocal Aubry-Andre model. This model features a coexistence of delocalized and Anderson localized states, and its Hamiltonian is given by [4]:

$$H = \sum_{j=1}^{L-1} \left((t + W_j) \hat{a}_j^\dagger \hat{a}_{j+1} + t \hat{a}_{j+1}^\dagger \hat{a}_j \right) + \sum_{j=1}^L V_j \hat{a}_j^\dagger \hat{a}_j, \quad (12)$$

where

$$\{W_j, V_j\} = \begin{cases} \{W, 2\lambda\} \cos(2\pi\alpha j + \theta), & j = n\kappa, \\ 0, & \text{else,} \end{cases} \quad (13)$$

with κ ($\kappa \leq 2$) an integer, λ the hopping coefficient, and θ the phase offset. Here, to induce SDC states, we introduce an irreciprocal hopping term

$$H_g = \sum_{j \neq n\kappa}^{L-1} (g \hat{a}_j^\dagger \hat{a}_{j+1} - g \hat{a}_{j+1}^\dagger \hat{a}_j). \quad (14)$$

Then the total Hamiltonian is $H + H_g$. The transfer matrices can be obtained as follows:

$$\begin{aligned} \mathcal{T}_i &= \begin{pmatrix} \frac{E}{1+g} & \frac{-(1-g)}{1+g} \\ 1 & 0 \end{pmatrix}^{\kappa-2} \begin{pmatrix} \frac{E}{1+g} & \frac{-1}{1+g} \\ 1 & 0 \end{pmatrix} \begin{pmatrix} \frac{E-V_j}{1+W_j} & \frac{-(1-g)}{1+W_j} \\ 1 & 0 \end{pmatrix} \\ &= \frac{1}{1+W_j} \begin{pmatrix} a_\kappa & -\alpha a_{\kappa-1} \\ a_{\kappa-1} & -\alpha a_{\kappa-2} \end{pmatrix} \begin{pmatrix} \frac{E^2 - EV_j - W_j - 1}{1+g} & \frac{-E(1-g)}{1+g} \\ E - V_j & -(1-g) \end{pmatrix}, \end{aligned} \quad (15)$$

where

$$\begin{pmatrix} \frac{E}{1+g} & \frac{-(1-g)}{1+g} \\ 1 & 0 \end{pmatrix}^{\kappa-2} = \begin{pmatrix} a_\kappa & -\alpha a_{\kappa-1} \\ a_{\kappa-1} & -\alpha a_{\kappa-2} \end{pmatrix}, \quad (16)$$

and a_κ is defined as

$$a_\kappa = \frac{1}{\Delta} \left[\left(\frac{\beta + \Delta}{2} \right)^{\kappa-1} - \left(\frac{\beta - \Delta}{2} \right)^{\kappa-1} \right], \quad (17)$$

with $\Delta = \sqrt{\beta^2 - 4\alpha}$, $\alpha = (1 - g)/(1 + g)$ and $\beta = E/(1 + g)$. Similar to the previous approach, we complexify the phase via the substitution $\theta \rightarrow \theta + i\epsilon$ and combine this transformation with Avila's global theory to obtain

$$\gamma(E) = \begin{cases} \max \left\{ \frac{1}{\kappa} \ln \left| \frac{2K_\kappa}{1 + \sqrt{1 - W^2}} \right|, 0 \right\}, & 1 \geq W, \\ \max \left\{ \frac{1}{\kappa} \ln \left| \frac{2K_\kappa}{W} \right|, 0 \right\}, & 1 < W, \end{cases} \quad (18)$$

where $K_\kappa = -Aa_\kappa + \alpha\lambda a_{\kappa-1}$ with $A = \frac{E\lambda + \frac{W}{2}}{1+g}$. When $\kappa = 2$ and $W > 1$, one can get that the mobility ring is determined by

$$\frac{1}{2} \ln \left| \frac{2E\lambda + W}{W(1 + g)} \right| = 0. \quad (19)$$

Figs. 3(a) to (c) display the eigenenergies marked by the fractal dimension Γ_n for the corresponding eigenstates for $g = (0.17, 0.2, 0.23)$, respectively, and a transition from localized states to critical states (with fractal structures) are found for the eigenstates in the enlarged insets [also for those with symmetric negative $\text{Im}(E)$]. In contrast to the model in the main text, here these states show SDC behaviors when their eigenenergies lie outside—yet in close proximity to—the mobility ring [those in panel (b)], as shown by the average scaling exponent β_{\min} and entanglement entropy \bar{S} in Figs. 3(d) and (e), respectively. In Fig. 3(c), the concerned eigenstates possess a loop-like spectrum and become conventional critical states.

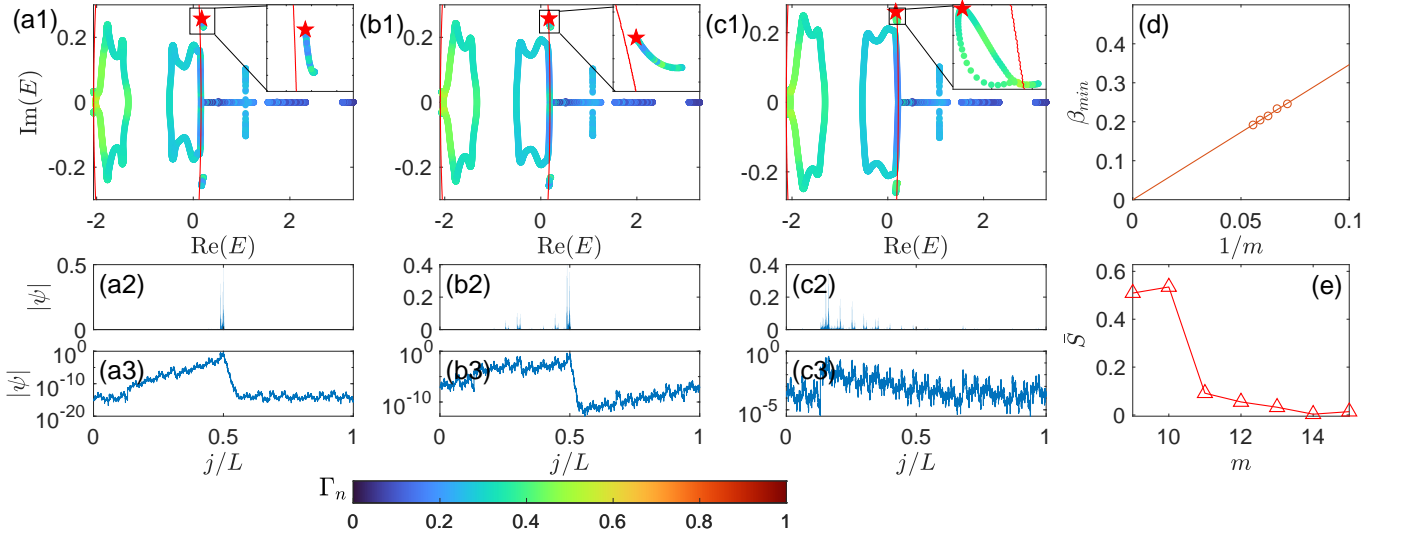


FIG. 3. (a1) to (c1) show the eigenenergies marked by the fractal dimension Γ_n for the corresponding eigenstates for $g = (0.17, 0.2, 0.23)$, respectively. The red curves represent the mobility rings obtained from Eq.(19). (a2) and (a3) show the wavefunctions of the local skin states corresponding to the red star in (a1). (b2) and (b3) show the wavefunctions of the SDC states corresponding to the red star in (b1). (c2) and (c3) show the wavefunctions of the conventional critical states corresponding to the red star in (c1). (d) and (e) present the multifractal analysis and the average entanglement entropy, respectively, of the SDC states for the parameter set used in (b). Other parameter are $W = 1.9$, $\lambda = 1$, $t = 1$ and $N = 1597$.

* lilinhu@quantumsc.cn

† xgf@sdu.edu.cn

- [1] X.-C. Zhou, Y. Wang, T.-F. J. Poon, Q. Zhou, and X.-J. Liu, Exact new mobility edges between critical and localized states, *Phys. Rev. Lett.* **131**, 176401 (2023).
- [2] A. Avila, Global theory of one-frequency Schrödinger operators, *Acta. Math.* **215**, 1 (2015).
- [3] K. Zhang, Z. Yang, and C. Fang, Correspondence between winding numbers and skin modes in non-hermitian systems, *Phys. Rev. Lett.* **125**, 126402 (2020).
- [4] S.-Z. Li, E. Cheng, S.-L. Zhu, and Z. Li, Asymmetric transfer matrix analysis of lyapunov exponents in one-dimensional nonreciprocal quasicrystals, *Phys. Rev. B* **110**, 134203 (2024).